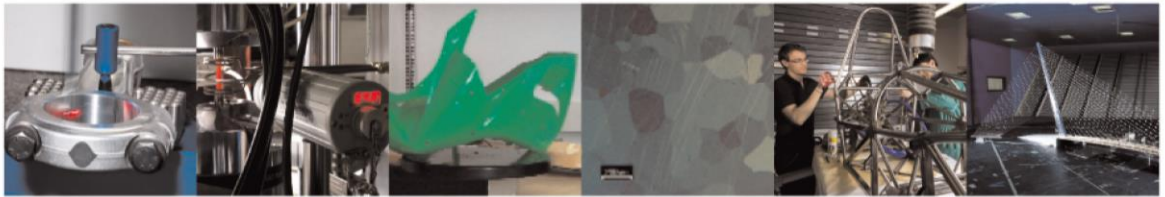




POLITECNICO
MILANO 1863

DIPARTIMENTO DI MECCANICA



Warping of FDM parts: Experimental tests and analytic model

Armillotta, Antonio; Bellotti, Mattia; Cavallaro, Marco

This is a post-peer-review, pre-copyedit version of an article published in ROBOTICS AND COMPUTER-INTEGRATED MANUFACTURING. The final authenticated version is available online at: <http://dx.doi.org/10.1016/j.rcim.2017.09.007>

This content is provided under [CC BY-NC-ND 4.0](https://creativecommons.org/licenses/by-nc-nd/4.0/) license



Warpage of FDM parts: experimental tests and analytic model

Antonio ARMILLOTTA^{1*}, Mattia BELLOTTI¹, Marco CAVALLARO²

¹ *Dipartimento di Meccanica, Politecnico di Milano, Milano, Italy*

² *Institute of Materials and Manufacturing, Brunel University, Uxbridge, UK*

* Corresponding author:

address: via La Masa 1, 20156 Milano, Italy

email: antonio.armillotta@polimi.it

tel.: +39 02 23998296

Abstract

Similarly to most additive manufacturing processes, Fused Deposition Modeling involves the processing of material by thermal cycles which can create distortions (warpage) in the built parts. The paper aims to characterize this defect on block-shaped parts in ABS thermoplastic resin as a function of some geometric variables related to the process: the size of the part in the three directions, and the thickness of deposited layers. For this purpose, the geometric deviations on parts manufactured with different combinations of the above variables have been measured and statistically analyzed in order to identify the influence factors and to estimate their individual and interaction effects on warpage. The results have given one main further insight compared to previous studies, namely the occurrence of a maximum distortion at intermediate values of part height. The attempt to explain it has suggested two additional hypotheses for the physical explanation of distortions: the extension of thermal stresses to multiple layers due to heat conduction from the last deposited layer, and the occurrence of bending stresses beyond the yield point of the material. These effects have been modeled by analytic equations in order to verify whether they can help improve the accuracy of warpage estimation.

Keywords

Fused deposition modeling, accuracy, shrinkage, thermal stress.

1 Introduction

Fused Deposition Modeling (FDM) is among the most widespread processes for the additive manufacturing (AM) of prototypes, tools and low-volume products. It consists in melting thermoplastic material by a vertical extruder and depositing it on a horizontal build platform, where it cools into a solid part. Due to the controlled relative motion of the extruder and the platform in the horizontal plane (x - and y -axis), an individual layer of the part is built as a continuous bead of deposited material. After a layer is completed, the platform is lowered along the vertical direction (z -axis) to allow the deposition of another layer, which welds to the previous one. The calculation of layer contours from a digital model of the part (slicing) is the basis for the generation of extrusion trajectories by appropriate programming software.

The increasing use of FDM for the manufacture of fixtures and functional parts is driving attention on the geometric accuracy of the process and on the related trade-offs with build time and cost. Depending on the application, specifications may be needed on FDM parts with regard to deviations from specified dimensions and geometric characteristics (e.g. form, orientation, surface profile), microgeometric errors (e.g. roughness), and build defects (e.g. delamination, voids, poor detail resolution). This paper deals with warpage, a geometric defect that is mostly observed on flat, thin parts and is usually explained as illustrated in Fig. 1. The material

extruded at melting temperature cools due to the large thermal gradient to surrounding air. This causes thermal contraction (shrinkage), which is prevented by the supporting platform and brings about tensile and compressive stresses throughout the part. At the end of the build, the part is removed from the platform and the stresses are released causing a bending distortion in the opposite direction of the former support reaction.

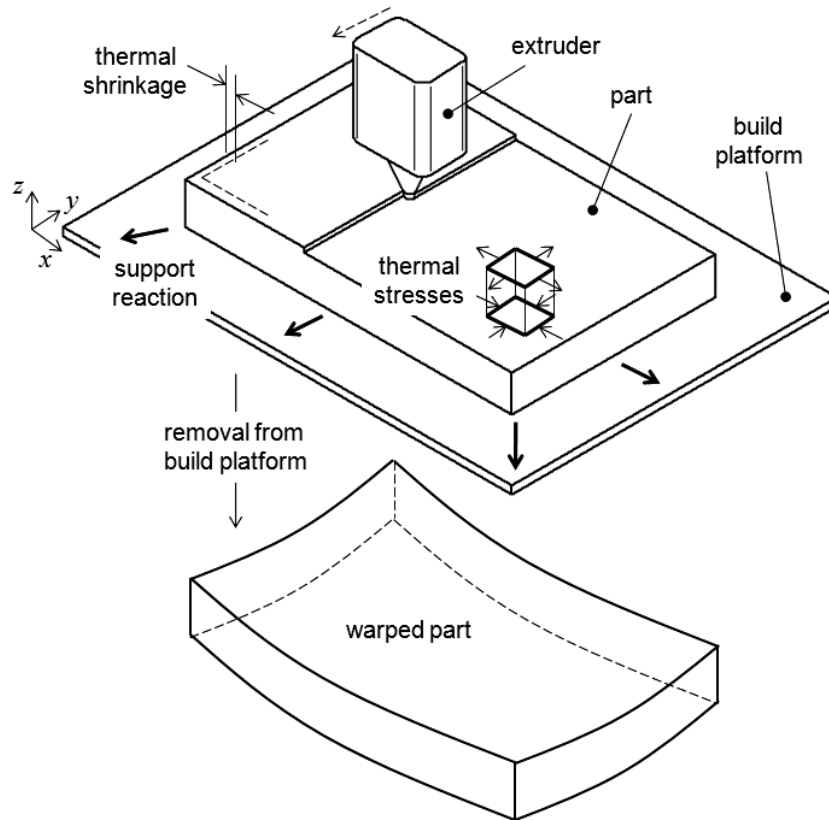


Fig. 1: Warpage in the FDM process

The above issue is known to be dependent on many variables related to material properties, part geometry and process parameters. In previous studies, analytic and simulation models have been developed to allow estimating the amount of warpage on parts with simple geometry for different combinations of influencing variables. Further developments seem to be needed for a full understanding of the specific mechanisms leading to warpage. Based on this objective, the paper reports some experimental tests focusing on the main geometric variables related to both the part (in-plane and vertical dimensions) and the process (layer thickness). The results of the tests show that some variables may have different effects to those highlighted in literature. Physical explanations are suggested for these effects, and their quantitative influence on warpage is evaluated by a simple analytic model.

The scope of the work is limited to parts with simple geometry (thin rectangular plates), made of a single material (acrylonitrile butadiene styrene, ABS) and built on an industrial-grade FDM machine. The latter assumption means that the process takes place within an enclosed chamber held at a proper temperature in order to keep shrinkage at a minimum. It is believed, however, that some insights of the work can be extended to different geometries (e.g. flat parts with complex profile), materials (e.g. polylactic acid, PLA) and machine types (low-end 3D printers with open workspace and possible heated platform).

2 Background

Recent reviews [1, 2] have discussed prior research efforts aimed to measuring, predicting and controlling different types of geometric errors on FDM parts. Compliance with geometric specifications has been clearly recognized as an additional criterion for process planning along with build time and cost [3].

Benchmark studies have initially focused on dimensional accuracy [4-8]. Deviations from specified dimensions have been shown to improve on recent industrial-grade machines [9-11] and low-end 3D printers [12, 13], and to depend on such process choices as (in decreasing order of importance) layer thickness, build orientation, deposition parameters, and the position of parts on the build platform [14-17]. With the increasing diffusion of international standards on geometric tolerancing, new benchmark parts have been proposed in order to measure form, orientation, position and profile errors [18-21].

The ability to compensate or control geometric errors requires further efforts to understand their possible causes. In [22-24], the positioning errors related to the machine are decomposed into translational and rotational components along different axes. Specific mechanisms highlighted for profile errors on part surfaces include the staircase effect due to the finite thickness of layers [25-27], perturbations on layer contours due to the raster scanning of the inside [28-30], systematic distortion on the topmost surfaces as an effect of finite-thickness slicing [31], and random distortion propagating from the substrate of support material [32].

Thermal shrinkage has been recognized as a key driver in several types of geometric errors. Experimental studies have focused on evaluating mean shrinkage for the compensation of dimensional errors [33] and post-shrinkage due to moisture [34], while less attention has been given to the anisotropy and random variation of shrinkage as it has been done on different AM processes [35]. In addition to available data on the coefficient of thermal expansion of FDM materials [36], some recent investigations have collected detailed measurements around glass transition temperature, where thermal contractions are more likely to determine residual stresses [37] and deformations [38] for the amorphous polymers usually processed by FDM.

Warpage has been initially observed as a visible effect of flatness errors in wide planar surfaces, measured by coordinate measuring machines on benchmark parts built by various AM processes including FDM [39]. Later on, flatness measurements have been mostly done by non-contact measuring instruments to avoid altering part geometry. Sensors embedded in the parts have been recently used to measure residual strains throughout the thermal history of the build process [40, 41].

Modeling approaches have been proposed in order to estimate the warpage of parts built with different process settings. They are invariably developed for thin rectangular plates to limit the complexity of describing equations and boundary conditions. The description of the process is usually based on the theory of thermoelasticity originally developed for the analysis of thermal stresses in structures (e.g. [42]), and always assumes the material elastic and isotropic with perfect bonding between layers. Different assumptions on the directions of shrinkage stresses lead to either one-, two- or three-dimensional models. They are usually verified by experimental tests, where the amount of warpage is measured on sample parts built with changing values of selected influencing variables.

In the 1D model of [43], the build process is analyzed in a planar vertical section, where the material is subjected to uniaxial stresses. The preferential orientation of the stress along the deposition trajectories and the heat transfer due to thermal gradients are neglected by assuming that the last layer is instantaneously deposited at melting temperature on the underlying layers at chamber temperature. The equilibrium of the forces and torques resulting from thermal stresses leads to an equation for the estimation of maximum part deflection, which is verified on a single part built by a FDM machine. More extensive experimental tests are reported in [44] with similar process settings, and in [45] on parts built by a low-end 3D printer.

The 2D model of [46] assumes that each point of the part is subjected to horizontal plane stress. Again, the last layer is assumed at constant temperature after instantaneous deposition. The classical equations of thermoelasticity for a thin plate (equilibrium, Hooke's law, and strain-displacement relationships) allow to develop an equation describing the deflection field in x - y . The estimation of warpage provided by the equation is verified on sample parts built by a low-end 3D printer.

The 3D model of [47] describes the onset of thermal stresses as a time-dependent process, which follows the motion of the extruder along deposition trajectories, and considers the heat transfer from the extruder position by conduction and convection. The coupled equations of equilibrium and energy conservation are solved by an iterative procedure implemented on commercial finite-element software. This results in a three-dimensional field of residual stresses, which allows to calculate part deflections after the removal from the build platform. Although it allows to capture transient effects of the process and compare different deposition strategies, the method requires a heavy computational effort, which limits its application to only small parts. The results of experimental tests on a FDM machine [48] are thus compared with regression values extrapolated from simulation results.

Warpage models of various complexity have been used for the multi-objective optimization of deposition parameters [49] and for a trajectory planning approach that is claimed to reduce distortion [50]. For other polymer-based AM processes, warpage has also been analyzed considering specific shrinkage effects as well as further process-dependent mechanisms; models and tests are reported for laser sintering [51-54], laser stereolithography [55-57], mask-projection stereolithography [58], and binder jetting [59].

Based on the available results, the variables with possible influence on warpage can be classified as related to:

- part geometry: length (l), width (w), height (h);
- material: coefficient of thermal expansion (α), Young's modulus (E), Poisson's ratio (ν), glass transition temperature (T_g);
- process: layer thickness (Δh), temperature of the heated chamber (T_c), deposition speed (v), height of the substrate of support material (h_s), deposition strategy (i.e. preferential orientation of beads).

Part geometry seems to be mostly influential on warpage, which is always reported to grow with increasing l and decreasing h , while the effect of w is less clearly defined. Among material properties, warpage is shown to be directly correlated with α , as well as to the temperature interval ($T_g - T_c$) where thermal shrinkage is known to generate stresses for amorphous polymers; a slight dependence on ν is also suggested by multi-dimensional models. Process-related factors are reported to have milder or controversial effects, with two notable exceptions: warpage increases slightly with Δh and if a long-raster filling strategy is chosen. In some studies, the analysis of experimental or simulation plans reveals significant interaction effects between variables, which are not usually discussed in detail.

This work builds on the above results with some specific questions and goals related to a subset of variables with geometric meaning (l , w , h , Δh). First, the inverse correlation with h suggests that warpage should raise special concerns for very thin parts, which is not consistent with the common experience with the process. Secondly, the choice of a suitable modeling approach (1D, 2D) depends on whether the effect of w is actually significant compared to random variation. Lastly, specific causes of influence need to be identified behind the correlation of warpage with each variable, in order to allow a future extension to more complex part geometries.

3 Material and methods

Samples of parts were built with the FDM process in order to measure the amount of warpage depending on part dimensions and layer thickness. All parts are rectangular plates with dimensions l and w in the horizontal plane (with $l \geq w$) and h in the build direction (Fig. 2a). The machine used for the tests is a Dimension Elite manufactured by Stratasys (Eden Prairie, MN), which can build parts with two different thicknesses Δh (0.178 and 0.254 mm). The build process is automatically driven by proprietary control software from an input file in STL format, which describes part geometry through a triangle mesh. The material used for the tests is a proprietary grade of ABS, commercially identified as ABSplus-P430 [60]. The parts are built layerwise upon a substrate made of SR10-P400SR soluble support material, an acrylic copolymer that is chemically removed by dipping the part into an alkaline aqueous solution at 75°C. The materials are deposited by two separate

extruders at $T_m = 270^\circ\text{C}$ (melting temperature) in a closed chamber held at a constant temperature $T_c = 75^\circ\text{C}$. Each layer is built first by contour offset, then by raster scanning of the inside area without leaving voids between roads (solid fill); the raster direction is at a 45° angle with the x - and y -axis of the machine, and changes by 90° rotation at each layer in order to reduce the mechanical anisotropy of the solidified polymer (Fig. 2b). The samples of parts were planned in advance and built in random sequences, possibly arranging multiple parts on the platform in a same build run; the position of a part on the platform was assumed as a disturbance factor along with other random causes of variation (e.g. machine conditions, material composition and handling, environmental conditions).

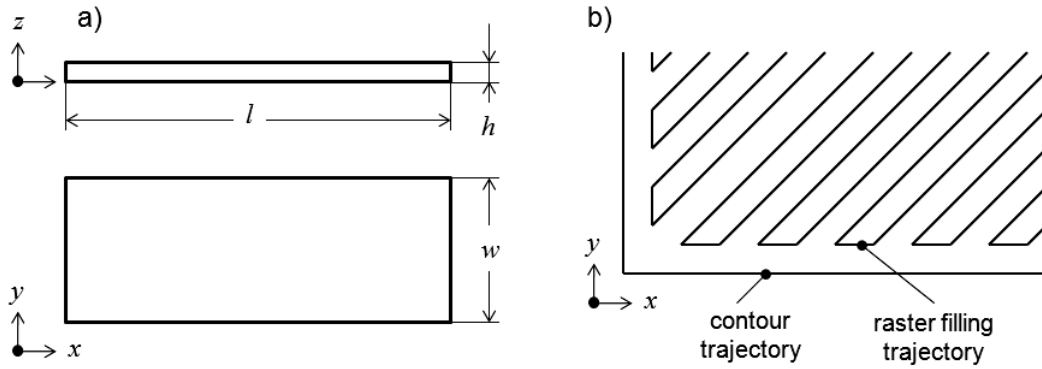


Fig. 2: Fabrication of sample parts: a) part geometry; b) deposition strategy

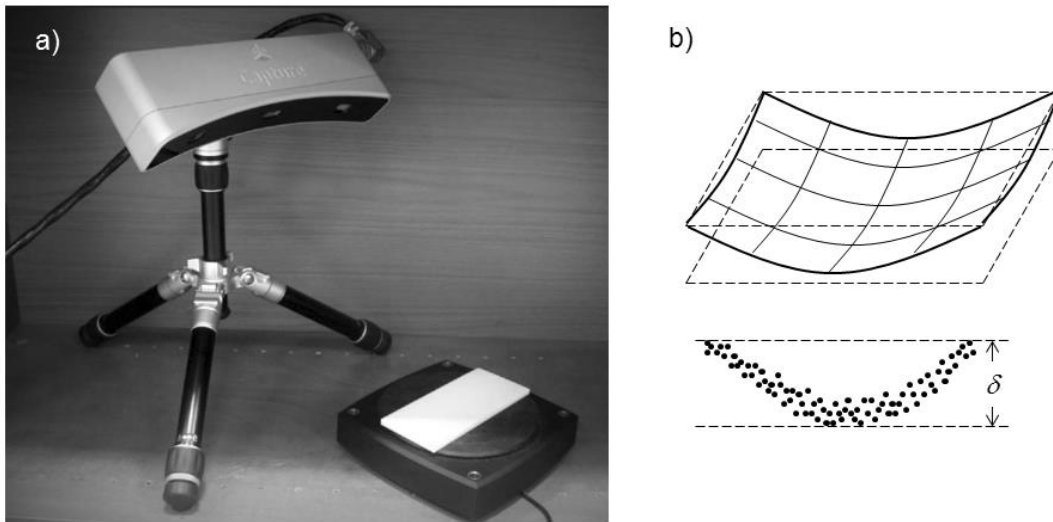


Fig. 3: Warpage evaluation: a) measurement of parts; b) flatness error

After extraction from the chamber and removal of supports, each part was inspected by the three-dimensional scanner Capture manufactured by 3D Systems (Rock Hill, SC). The instrument is based on the blue LED light scanning technology and measures point coordinates at distances in the 300-600 mm range at an accuracy estimated around $60\ \mu\text{m}$ for the adopted measuring setup (Fig. 3a). For each part, a point cloud with spacing around $0.15\ \text{mm}$ was collected on the rectangular surface facing upward during the build process (number of points between 10k and 90k depending on part size $l \times h$). The point cloud was then analyzed by a specifically developed software procedure, which allows the visual diagnosis of possible scanning errors and calculates the amount of warpage. The latter is expressed by the flatness error δ , defined as the minimum distance between two parallel planes containing the whole point set (Fig. 3b). The orientation of such planes was calculated by fitting the point set through the iterative MinMax algorithm [61], starting from an initial solution given by the least-square plane of the points. The flatness error can be directly compared with the maximum deflection calculated in some analytic methods in literature. The scan and the related data processing

were repeated twice for each part, checking the variation of results against the stated accuracy of the instrument, and eventually assigning an averaged value of flatness error to the part.

The experiments for the evaluation of warpage were designed as full factorial plans [62]. Each plan includes a set of variables (factors), each taking a discrete set of values (levels). The flatness error δ (response) is evaluated under all combinations among factor levels. Multiple values of the response (replications) are gathered for each combination in order to evaluate the random variation due to disturbances. The influences of the factors on the response through individual and interaction effects is then statistically tested by the analysis of variance (ANOVA), which is based on approximating the data by a best-fit linear model. To validate the results of the ANOVA, the deviations of the data from the model (residuals) are statistically tested for normality, homogeneity of variance, and lack of autocorrelation.

4 Experimental results

The set of factors considered in this work includes three variables related to part geometry (l , w , h) and one related to process planning (Δh). It was thought that a first screening of part-related factors could be helpful before including the process-related factor in the analysis. Therefore, a first experiment was conducted at constant layer thickness, resulting in the selection of a subset of part dimensions with significant influence on warpage. In a second experiment, the selected set of factors was tested with different layer thicknesses.

4.1 First experiment: part dimensions

Tab. 1 shows the design of the first factorial plan focused on part-related factors. Layer thickness Δh was set to 0.254 mm, a default value preferred in many applications of the FDM process to achieve a good compromise between surface finish and build time. Length l was varied in three levels, covering a wide range of sizes (60-140 mm) regarded as interesting for applications and visual impact of warpage. Width w was tested in two levels over a lower range of values (20-60 mm), so that its meaning could not be confused with length. Three levels were selected for height h , from a minimum expected for common applications (1.5 mm) to a maximum close to those suggested in literature as critical for warpage (5.5 mm). Each of the 18 combinations of factor levels was replicated twice (two parts separately built and measured), resulting in 36 values of response δ collected in random sequence. The results of the plan are reported in Tab. 2.

Tab. 1: Factors and levels of the first experiment

<i>Factor</i>	<i>Unit</i>	<i>Levels</i>
l	mm	60 100 140
w	mm	20 60
h	mm	1.5 3.5 5.5
Δh	mm	0.254

Tab. 3 shows the ANOVA of δ with respect to l , w and h . The total variation of the response is decomposed in a random error and in 7 individual and interaction effects of the three factors. The significance of each effect is verified by an F-test, whose statistic is calculated from the number of available independent values of the source (degrees of freedom, DOF) and by a measure of the response differences that can be assigned to the source (sum of squares, SS). A higher value of F correspond to a lower probability of rejecting the hypothesis that the related effect occurs (p-value). The effect is significant if such probability is lower than a preset confidence level (e.g. 1.5% for individual tests, corresponding to about 10% for the whole family of 7 tests). The relevance of a significant effect is related to the value of SS, which contributes additively to total variation. The result of the ANOVA suggests that w does not significantly influence the amount of warpage, while l and

h have both individual and interaction effects. The most relevant effect is that of l , which explains nearly 95% of total variation. The validity of the ANOVA was confirmed by the tests on residuals as regards normal distribution ($p = 0.404$ in the Anderson-Darling test), homogeneity of variance ($p = 0.976$ in the Bartlett's test, no abnormal differences among the 95% Bonferroni confidence intervals of variances), as well as lack of autocorrelation and abnormal trends with respect to either the factors and the fitted values of the response.

Tab. 2: Warpage measured with different combinations of part dimensions

l [mm]	w [mm]	h [mm]	δ [mm]	δ [mm]
60	20	1.5	0.36	0.39
60	20	3.5	0.46	0.43
60	20	5.5	0.44	0.39
60	60	1.5	0.37	0.40
60	60	3.5	0.51	0.52
60	60	5.5	0.47	0.43
100	20	1.5	0.58	0.58
100	20	3.5	0.69	0.65
100	20	5.5	0.64	0.71
100	60	1.5	0.58	0.51
100	60	3.5	0.70	0.67
100	60	5.5	0.65	0.67
140	20	1.5	0.93	0.92
140	20	3.5	1.02	1.07
140	20	5.5	0.97	0.96
140	60	1.5	1.06	1.08
140	60	3.5	1.00	0.97
140	60	5.5	0.91	0.94

Tab. 3: ANOVA of warpage with respect to part dimensions

Source	DOF	SS	F	p
l	2	1.88042	1502.14	0.000
w	1	0.00144	2.29	0.147
h	2	0.03435	27.44	0.000
$l * w$	2	0.00421	3.37	0.057
$l * h$	4	0.02885	11.52	0.000
$h * w$	2	0.00345	2.75	0.090
$l * w * h$	4	0.02569	10.26	0.000
Error	18	0.01127		
Total	35	1.98698		

Fig. 4 shows the plots of the individual effects, i.e. the average response values at the different levels of the factors; the mean-connecting line is shown for visual effectiveness and does not imply interpolation of values between levels. Again, it can be noted that δ is mostly influenced by l while the effect of h is less relevant and the effect of w clearly negligible. Given the high repeatability of the response within factor levels, the trends in the plots of l and h seem to suggest nonlinear effects of the two factors: the amount of warpage seems to increase more than linearly with length, and seems to have a maximum for intermediate values of height. According to the plots of interaction effects, not shown in figure, in no case does the effect of a factor

significantly depend on the values of other factors, which would have suggested functional relationships between variables.

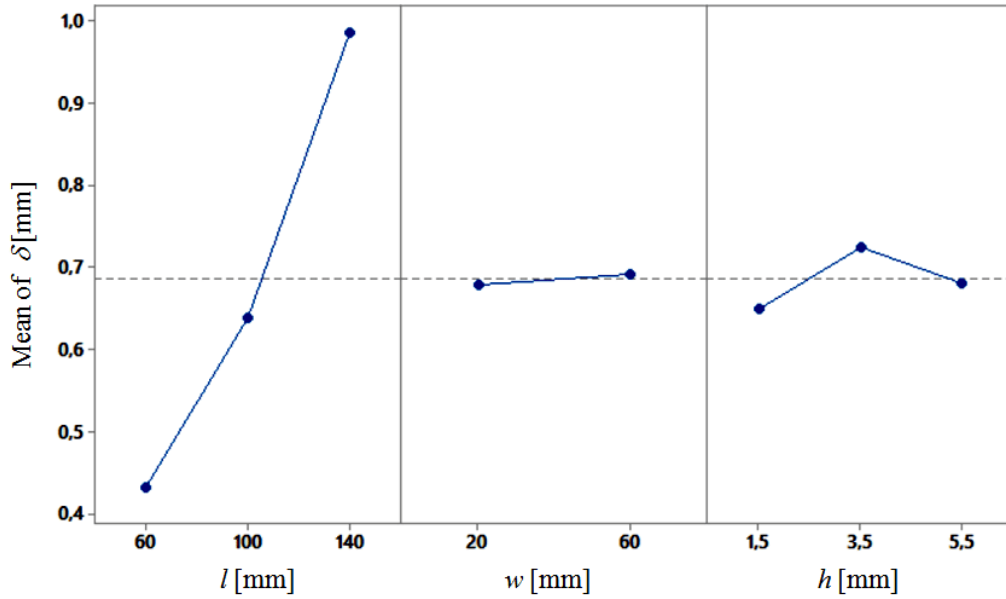


Fig. 4: Individual effects of part dimensions

4.2 Second experiment: selected part dimensions and layer thickness

Tab. 4 shows the design of the second factorial plan. Considering the above results, width w was excluded from further investigation and set to the lowest value among those previously tested. The same values as in the first experiment were set for the remaining dimensions, except for a further level of length l (20 mm) added to verify the nonlinearity of the related effect. Thickness Δh was varied in the two values available on the machine, thus adding the setting preferred for parts with special surface quality (0.178 mm). The plan has 24 combinations of factor levels, each replicated twice for a total of 48 values of the response δ , among which 18 values already collected in the common settings of the first experiment. The results of the plan are reported in Tab. 5.

Tab. 4: Factors and levels of the second experiment

<i>Factor</i>	<i>Unit</i>	<i>Levels</i>
l	mm	20 60 100 140
w	mm	20
h	mm	1.5 3.5 5.5
Δh	mm	0.178 0.254

The ANOVA of the response, shown in Tab. 6, suggests that all factors have significant effects both individually and in pairwise interaction. The most relevant effect is again that of l , which accounts for about 90% of the total variation of δ . The remaining variation is accounted for in nearly equal way by the individual effects of h and Δh , and by the interaction between l and h . The residuals have normal distribution ($p = 0.348$ in the Anderson-Darling test), homogeneous variance ($p = 0.994$ in the Bartlett's test, no abnormal differences among the 95% Bonferroni confidence intervals of variances), and lack of autocorrelation and abnormal trends, thus confirming the validity of the analysis.

Tab. 5: Warpage measured with varying length, height and layer thickness

l [mm]	h [mm]	Δh [mm]	δ [mm]	
20	1.5	0.178	0.21	0.16
20	1.5	0.254	0.20	0.24
20	3.5	0.178	0.23	0.27
20	3.5	0.254	0.27	0.26
20	5.5	0.178	0.17	0.19
20	5.5	0.254	0.24	0.22
60	1.5	0.178	0.27	0.30
60	1.5	0.254	0.36	0.39
60	3.5	0.178	0.34	0.35
60	3.5	0.254	0.46	0.43
60	5.5	0.178	0.28	0.26
60	5.5	0.254	0.40	0.39
100	1.5	0.178	0.56	0.60
100	1.5	0.254	0.61	0.58
100	3.5	0.178	0.55	0.52
100	3.5	0.254	0.69	0.65
100	5.5	0.178	0.50	0.47
100	5.5	0.254	0.64	0.71
140	1.5	0.178	0.91	0.94
140	1.5	0.254	0.93	0.92
140	3.5	0.178	0.82	0.85
140	3.5	0.254	1.02	1.07
140	5.5	0.178	0.71	0.71
140	5.5	0.254	0.97	0.98

Tab. 6: ANOVA of warpage with respect to length, height and layer thickness

Source	DOF	SS	F	p
l	3	3.03618	1942.18	0.000
h	2	0.09505	91.20	0.000
Δh	1	0.06314	121.18	0.000
$l * h$	6	0.06579	21.04	0.000
$l * \Delta h$	3	0.00981	6.27	0.003
$h * \Delta h$	2	0.00970	9.31	0.000
$l * h * \Delta h$	6	0.01018	3.26	0.017
Error	24	0.01251		
Total	47	3.30235		

The plots of individual effects in Fig. 5 seem to confirm that the amount of warpage grows more than linearly with length, and has a maximum for intermediate values of height. They also show that thicker layers lead to slightly higher warpage. The interactions (plots not shown) are far less relevant and would require further verification on wider experimental plans, yet they give a few additional cues: with thicker layers, the distortions grow less rapidly with length and the peak at intermediate height is more pronounced.

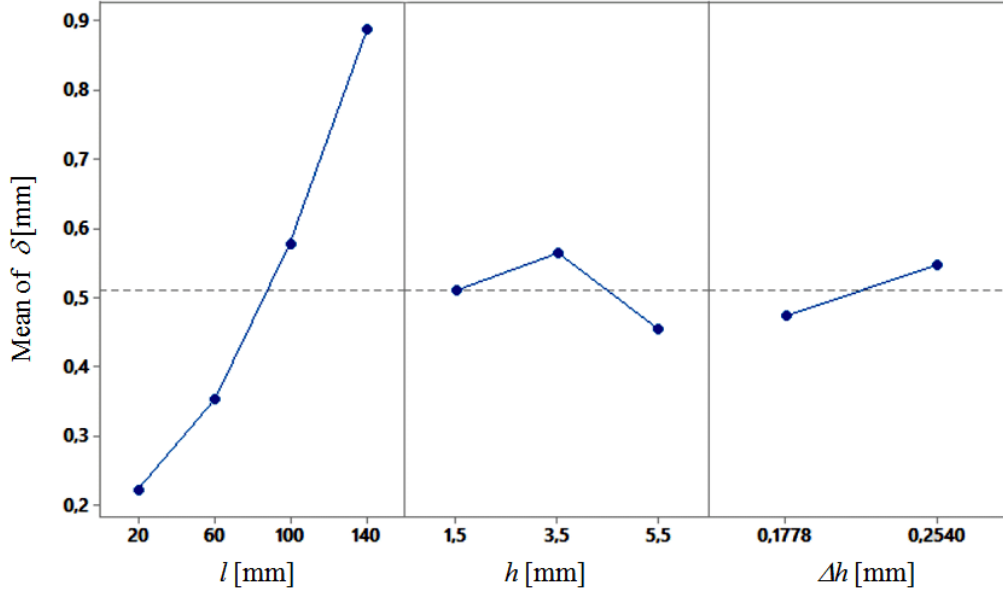


Fig. 5: Individual effects of length, height and layer thickness

5 Interpretation

Some effects noted in the experimental tests are different from those already pointed out in literature. The most evident case relates to Δh , which seems to have a critical range somewhere between 2 and 4 mm (more levels would be required for a tighter bracketing of the maximum) whereas previous studies had shown an inverse correlation of warpage with layer thickness. This inconsistency might depend on physical mechanisms not yet discussed in the explanation of accuracy issues in the FDM process.

A simplified explanation of how warpage occurs, consistent with the assumptions of analytic models in literature, is illustrated in Fig. 6. A new layer of material is instantaneously deposited at melting temperature T_m on a substrate (the part built so far) at chamber temperature $T_c < T_m$, and is subjected to thermal contraction while it cools. The platform counteracts the shrinkage of the layer by reaction forces on the bottom plane of the part. The torque of such forces with respect to the midplane of the part leads to elastic stresses, which result into residual bending deformation once the part is removed from the platform.

If only the shrinkage along the direction of length is considered, the part is subjected to uniaxial stress depending on the vertical position. The thermal stress in the new layer

$$\sigma = E\alpha(T_g - T_c)$$

is caused by the reaction force of the platform:

$$F = E\alpha(T_g - T_c)w\Delta h \quad (1)$$

whose lever arm with respect to the midplane of the part gives the bending moment

$$M = F \frac{h - \Delta h}{2} = \frac{1}{2} E\alpha(T_g - T_c)wh\Delta h \left(1 - \frac{\Delta h}{h}\right) \quad (2)$$

As long as the part is in the build process, M keeps it straight on the platform. Once it is removed from the constraint, the part bends as if it were loaded by a bending moment $-M$. The elastic deflection at midspan is

$$\delta_T = \frac{Ml^2}{8EJ} = \frac{1}{2} E\alpha(T_g - T_c)wh\Delta h \left(1 - \frac{\Delta h}{h}\right) \frac{l^2}{8E} \frac{12}{wh^3} = \frac{3}{4} \alpha(T_g - T_c) \frac{l^2 \Delta h}{h^2} \left(1 - \frac{\Delta h}{h}\right) \quad (3)$$

where J is the second area moment of the cross section of the part. If $\Delta h / h \ll 1$, it can be easily verified that equation (3) is identical to the expression of deflection found in [43]:

$$\delta_T = \frac{n^3 \Delta h}{6\alpha(T_g - T_c)(n-1)} \left[1 - \cos\left(\frac{3\alpha l}{n\Delta h}(T_g - T_c)\frac{n-1}{n^2}\right) \right]$$

where $n = h / \Delta h$ is the number of layers, once the cosine is replaced by its second-order Taylor expansion (the argument is small enough that further terms can be neglected).

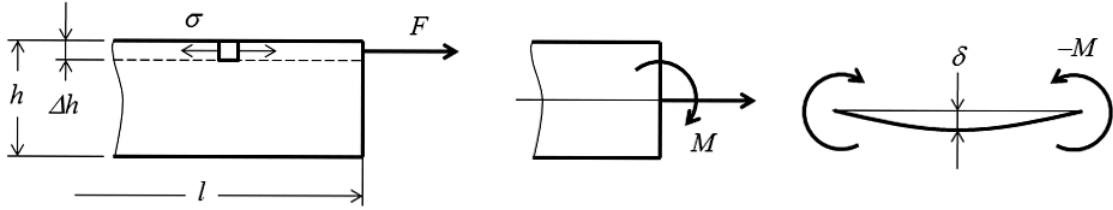


Fig. 6: One-dimensional illustration of warpage

According to this simple analytic model, the amount of warpage increases more than linearly with l , is proportional to Δh and decreases monotonically with increasing h . These relationships can be compared with the effects illustrated in Fig. 5, in order to get an intuitive feel for the causes of influence of each variable, trying to explain the inconsistencies with further hypotheses.

The tests confirm that warpage grows more than linearly with l . This is simply what is expected for a beam subjected to constant bending moment. No further explanation of the influence of part length needs thus to be looked for.

Similarly, the observation that warpage does not actually depend on w seems to be fully explained by the balance of two conflicting causes. A wider part is subjected to thermal stresses over a larger volume, and thus to a higher bending moment. On the other hand, it has a higher bending stiffness: as a result, its deflection does not increase. A deeper analysis would consider that warpage occurs in the direction of width too; although this should lead to an increased flatness error, the contribution of w is likely to be negligible compared to l because of the dependence of deflection with the square of the dimension.

The actual influence of h is in contrast with equation (3), as warpage seems to have a maximum instead of a monotonic correlation with height. The behavior for relatively large values of h can be explained considering that, when the height decreases, the bending stiffness decreases more rapidly than the bending moment increases, which results into a larger deflection. Below a certain height, however, this explanation is no longer sufficient. Two additional hypotheses can thus be formulated:

1. The heat input to the part due to the deposition of a new layer at temperature T_m is transferred to the chamber at temperature T_c both by convection to surrounding air and by conduction to the substrate. A thermal transient thus occurs in the underlying layers, whose temperature raises from T_c to a peak value T_{max} and then falls again to T_c . Some layers can reach a peak temperature $T_{max} > T_g$, and thus shrink again as they cool down. If this occurs, the deposition of a new layer creates thermal stresses also in some of the underlying layers; the total tensile force due to constrained shrinkage has thus a smaller lever arm with respect to the midplane of the part (Fig. 7). As an extreme case, it may even happen that all layers shrink at each thermal transient, and the bending moment drops to zero. More realistically, it is reasonable to expect that at small part heights the bending moment decreases more rapidly than the bending stiffness, with a consequent reduction of warpage.
2. As said before, the warpage of a part occurs in two phases: first, the reaction torque M of the platform prevents the thermal deformation due to shrinkage; then, the part is removed from the platform and bends as if it were subjected to a torque $-M$. If the bending stress in the first phase is lower than the yield point of the material, as it has been assumed until now, M keeps the part straight without

deforming it permanently, i.e. the thermal deflection δ_T is completely elastic (Fig. 8a). Should instead the bending stress exceed the yield point, the part would have to withstand a permanent deflection δ_P in the opposite direction (i.e. in the direction of straightening the part) in addition to the elastic deflection δ_M due to the reaction torque (Fig. 8b). Once the constraint is removed, the part would only recover the elastic component δ_M of the deformation, thus the residual deflection $\delta_R = \delta_T + \delta_P$ would be smaller than with only elastic stresses. As the elastic deflection δ_T grows rapidly when h decreases, the onset of permanent deformation is especially likely for parts with small height and may contribute to explain the smaller deflections observed in practice.

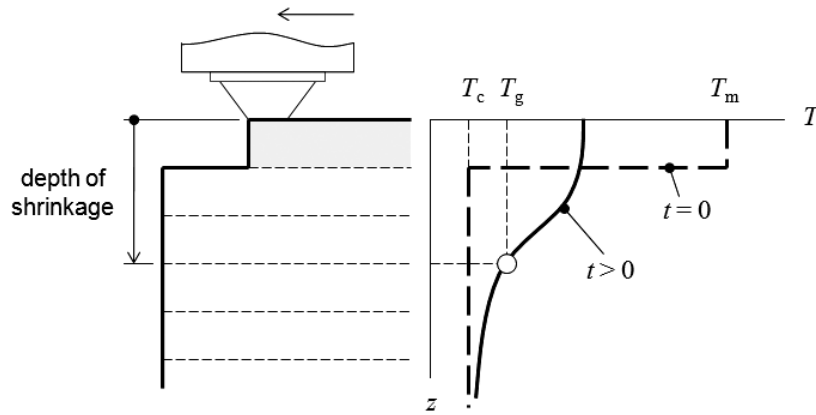


Fig. 7: Shrinkage on multiple layers

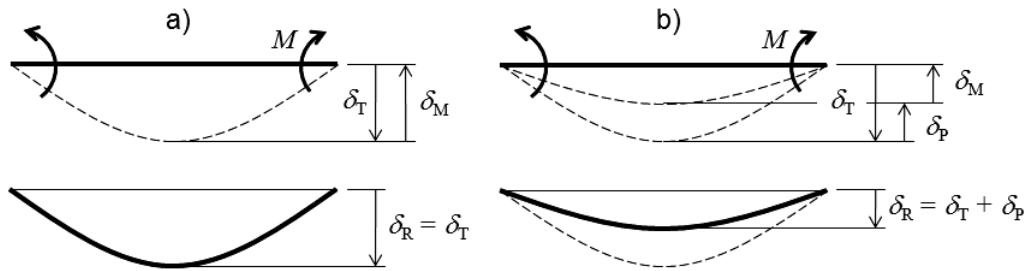


Fig. 8: Development of warpage after build: a) with elastic deformation; b) with permanent deformation

Lastly, the tests confirm that warpage increases with Δh ; according to the simplified analytic model, this is because thicker layers involve thermal stresses on a larger volume and thus a larger reaction force from the platform. However, the slope of δ in the individual effect plot of Δh suggests that the deflection is actually not proportional to the thickness as the model would predict. Such an inconsistency, which would have to be verified by further tests, seems to be consistent with the hypothesis of multiple-layer shrinkage. If the layer thickness were set to a very low value, the heat input would be so small that very little conduction would occur to the underlying layers. This would reduce the amount of material undergoing shrinkage and thus a more rapid decrease of warpage. It should also be noted that the flatness error measured in the tests may include a minor contribution not related to warpage, the depth of the small grooves in the top plane due to the curved free boundary of the deposited beads (usually referred to as roughness), which is expected to increase with layer thickness.

The proposed hypotheses about the warpage of thin parts seem to be in accordance with known material and process properties. About multiple-layer shrinkage, the chance that a relevant share of the heat input is conducted to underlying layers can be expected from the values assumed by previous studies (e.g. [63]) for the thermal conductivity ($k = 0.18 \text{ W/m}^2\text{K}$) and for the convective heat transfer coefficient ($c = 30 \text{ W/mK}$). For a part with $h = 0.003 \text{ m}$, the transient heat transfer problem would have a relatively small value of the Biot

number, the dimensionless group representing the relative importance of convection with respect to conduction:

$$\text{Bi} = \frac{ch}{k} \approx 0.5$$

The occurrence of plastic deformation is not usually taken into consideration, as the amorphous polymers at room temperature have a relatively brittle (glassy) behavior. Yet at temperatures close to T_g it is reasonable to expect a partial transition to a rubbery behavior, which for linear polymers does not involve complete elastic recovery of deformation due to relative sliding of polymer chains [64]. Furthermore, ABS has special properties due to the presence of butadiene units, which give the copolymer a first partial glass transition at -50°C . This makes it partially rubbery even at room temperature, as witnessed by the 6-8% elongation at break measured on FDM tensile specimens in the whole range of temperatures below T_g [65]. Although more data on the mechanical properties of ABS at high temperature would be needed to collect more evidence, the above considerations seem to be consistent with the idea of thermal stresses beyond the elastic range.

6 Analytic modeling

The two proposed hypotheses are now developed in order to verify whether they can actually explain the observed influence of part height on warpage.

6.1 Multiple-layer shrinkage

A new layer deposited at temperature T_m cools quickly to the temperature T_c of both the build chamber and the substrate. During the thermal transient, a few underlying layers are re-heated by conduction and their temperature exceeds T_g again. This cancels the previous thermal stress and creates new shrinkage in the following cooling to T_c . As the shrinkage stresses are located in an extended layer of material with thickness $h_0 > \Delta h$, they induce an increased bending moment and thus a larger elastic deformation.

A first-approximation evaluation of h_0 can be done by the simple heat transfer model illustrated in Fig. 9. A semi-infinite plate in direction Z has initial constant temperature T_c , and receives at time $t = 0$ a finite amount H of heat per unit area on its boundary plane at $Z = 0$. The evolution of temperature $T(Z, t)$ satisfies the heat transfer equation

$$\rho c_p \frac{\partial T}{\partial t} = k \frac{\partial^2 T}{\partial Z^2}$$

and, neglecting the convective cooling, the following boundary conditions:

$$\begin{aligned} Z = 0: & -k \frac{\partial T}{\partial Z} = 0 \\ Z \rightarrow \infty: & T = T_c \\ t = 0: & T = T_c \\ \int_0^\infty \rho c_p (T - T_c) dZ & = H \end{aligned}$$

where k [W/m²K], ρ [kg/m³] and c_p [J/kgK] are the thermal conductivity, density and specific heat capacity of the material. The above problem has the following analytic solution [66]:

$$T = T_c + \frac{H}{\rho c_p} \frac{1}{\sqrt{\pi k t}} \exp\left(-\frac{Z^2}{4 k t}\right)$$

where $\kappa = k / \rho c_p$ is the thermal diffusivity of the material [m²/s]. If the plate corresponds to an FDM part with a sufficiently high $h / \Delta h$ ratio, the heat input by the deposition of the last layer is

$$H = \rho c_p \Delta h (T_m - T_c)$$

and thus

$$T = T_c + (T_m - T_c) \frac{\Delta h}{\sqrt{\pi \kappa t}} \exp\left(-\frac{Z^2}{4 \kappa t}\right)$$

The above equation allows to calculate the depth Z of the layer that reaches T_g at time t :

$$T = T_g \rightarrow Z = 2\sqrt{\kappa} \sqrt{t} \sqrt{\ln\left(\frac{\Delta h}{\sqrt{\pi \kappa}} \frac{T_m - T_c}{T_g - T_c}\right) - \ln \sqrt{t}}$$

The maximum depth h_0 is given by the condition

$$\frac{dZ}{dt} = 0 \rightarrow \sqrt{t} = \frac{\Delta h}{\sqrt{\pi \kappa}} \frac{T_m - T_c}{T_g - T_c}$$

and is equal to

$$h_0 = Z = 2\sqrt{\kappa} \frac{\Delta h}{\sqrt{\pi \kappa}} \frac{T_m - T_c}{T_g - T_c} \sqrt{\ln\left(\frac{\Delta h}{\sqrt{\pi \kappa}} \frac{T_m - T_c}{T_g - T_c}\right) - \ln \frac{\Delta h}{\sqrt{\pi \kappa}} \frac{T_m - T_c}{T_g - T_c}} = \Delta h \cdot \sqrt{\frac{2}{\pi} \frac{T_m - T_c}{T_g - T_c}}$$

It results that the height of the volume subjected to shrinkage is proportional to layer thickness:

$$h_0 = m \Delta h, \quad m = \sqrt{\frac{2}{\pi} \frac{T_m - T_c}{T_g - T_c}} \approx 0.5 \frac{T_m - T_c}{T_g - T_c} \quad (4)$$

The parameters commonly assumed for ABS ($T_m = 250\text{-}300^\circ\text{C}$, $T_g = 90\text{-}110^\circ\text{C}$, $T_c = 70\text{-}80^\circ\text{C}$) give values of m between 4 and 5, hence the deposition of a layer causes shrinkage in the 3-4 underlying layers as well. This result is only valid for high $h / \Delta h$ ratios and neglects the convective cooling through the top plane. However, it has been verified that m decreases by less than 5% when numerically solving equivalent heat transfer models on plates with finite height $h > 1.5$ mm, common choices of layer thickness ($\Delta h = 0.178$ and 0.254 mm), and with convective heat transfer coefficients $c = 5\text{-}30$ W/mK (suggested range for convection in forced air at low speeds). For smaller heights, actually not interesting for applications, numerical simulations show that $h_0 \approx h$.

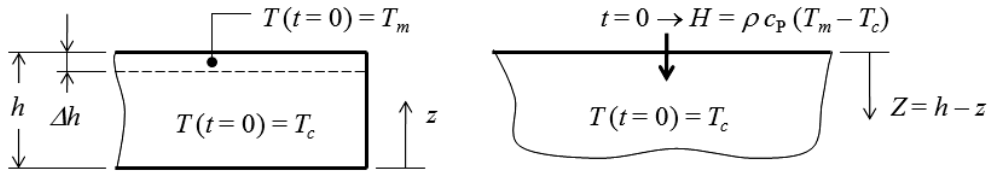


Fig. 9: Heat transient model for the calculation of shrinkage volume thickness

If the thermal stress is in the elastic range, the deflection due to warpage can be calculated by replacing Δh with h_0 in equation (3):

$$\delta_T = \frac{3}{4} \alpha (T_g - T_c) \frac{l^2 h_0}{h^2} \left(1 - \frac{h_0}{h}\right) = \frac{3}{4} \alpha (T_g - T_c) \frac{l^2 m \Delta h}{h^2} \left(1 - \frac{m \Delta h}{h}\right) \quad (5)$$

6.2 Plastic deformation

If the material is stressed beyond the elastic range, and assuming that the part does not lose contact with the platform, the deflection of the part during the process is

$$\delta_T + \delta_M + \delta_p = 0$$

that is, a free part would naturally bend due to shrinkage (thermal deflection $\delta_T > 0$), but the platform counter-bends the part elastically (elastic deflection $\delta_M < 0$) and then plastically (permanent deflection $\delta_p < 0$). The torque M of the support reaction is only related to the elastic stresses, while the plastic stresses do not require any further force to develop. When the part is detached from the platform, the support reaction vanishes, and the residual deflection of the part is

$$\delta_R = \delta_T + \delta_p = -\delta_M$$

The actual deflection of the part is less than what would be expected under the elastic assumption, and equals the deflection of a free part subjected to a torque $-M$. To calculate M , the stresses limited by the yield point have to be evaluated and integrated over the height of the part.

By extending equations (1) and (2) to the assumption of multiple-layer shrinkage, the thermal stresses have a resultant torque

$$M = \frac{1}{2} E \alpha (T_g - T_c) w h_0 h \left(1 - \frac{h_0}{h} \right)$$

which corresponds to a linear stress pattern with maximum value

$$\sigma_{\max} = \frac{Mh}{2J} = \frac{1}{2} E \alpha (T_g - T_c) w h_0 h \left(1 - \frac{h_0}{h} \right) \frac{h}{2} \frac{12}{wh^3} = 3E\alpha(T_g - T_c) \frac{h_0}{h} \left(1 - \frac{h_0}{h} \right)$$

In addition, the pulling force

$$F = E \alpha (T_g - T_c) w h_0$$

induces the tensile stress

$$\sigma_n = \frac{F}{A} = \frac{E \alpha (T_g - T_c) w h_0}{wh} = E \alpha (T_g - T_c) \frac{h_0}{h}$$

The maximum total stress is thus

$$\sigma_{\max} + \sigma_n = 3E\alpha(T_g - T_c) \frac{h_0}{h} \left(\frac{4}{3} - \frac{h_0}{h} \right)$$

If the material has a yield point σ_Y , there is tensile yielding if

$$\sigma_{\max} + \sigma_n > \sigma_Y \rightarrow \frac{\sigma_Y}{E \alpha (T_g - T_c)} < 3 \frac{h_0}{h} \left(\frac{4}{3} - \frac{h_0}{h} \right)$$

and compressive yielding if

$$-\sigma_{\max} + \sigma_n < -\sigma_Y \rightarrow \frac{\sigma_Y}{E \alpha (T_g - T_c)} < 3 \frac{h_0}{h} \left(\frac{2}{3} - \frac{h_0}{h} \right)$$

The parameter

$$a = \frac{\sigma_Y}{E\alpha(T_g - T_c)} \quad (6)$$

depends on the thermo-mechanical properties of the material in the temperature interval between T_g and T_c . Reasonable ranges for these properties ($\alpha = 40\text{-}80 \cdot 10^{-6} \text{ K}^{-1}$, $E = 1000\text{-}2000 \text{ MPa}$, $\sigma_Y = 1\text{-}2 \text{ MPa}$) can be assumed from published data for ABS [60] and suggest that a might take values between 0.5 and 2. Considering the relation between h_0 and Δh given by equation (4), tensile yielding is thus expected for a wider and wider range of $h / \Delta h$ ratios as a decreases. Compressive yielding is highly unlikely and will not be considered in the following.

Assuming that the material is perfectly plastic, the stress σ is limited by σ_Y but its variation along part thickness is more difficult to calculate than under the elastic assumption. This makes it difficult to separate the elastic and plastic contributions to part deflection unless a further simplification is introduced. For instance, the stress pattern can be regarded as a plain yield-limited version of the elastic one as shown in Fig. 10. Along a reference axis ζ with origin at the middle plane of the part, the yield point is reached at a coordinate ζ_0 given by

$$\frac{2\sigma_{\max}\zeta_0}{h} + \sigma_n = \sigma_Y \rightarrow \zeta_0 = \frac{\sigma_Y - \sigma_n}{\sigma_{\max}} \frac{h}{2}, \quad \frac{\sigma_Y - \sigma_n}{\sigma_{\max}} < 1 \quad (7)$$

and $\sigma = \sigma_Y$ for $\zeta \geq \zeta_0$. The torque of the stresses on the whole section around the neutral axis of bending ($\zeta = 0$) can be calculated as

$$M_R = M - M_p \quad (8)$$

where M_p is the integral of the elastic stresses that exceed the yield point, and are thus responsible for the permanent counter-bending of the part. Again with reference to Fig. 10, it results that

$$M_p = w \cdot \frac{1}{2} \left(\frac{h}{2} - \zeta_0 \right) (\sigma_{\max} + \sigma_n - \sigma_Y) \cdot \left[\zeta_0 + \frac{2}{3} \left(\frac{h}{2} - \zeta_0 \right) \right]$$

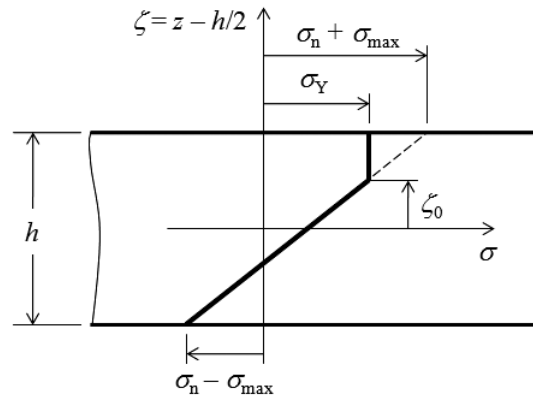


Fig. 10: Simplified stress pattern in the presence of plastic deformation

From equation (7) and remembering that

$$\sigma_{\max} = \frac{Mh}{2J} = \frac{6M}{wh^2}$$

simple passages lead to

$$M_p = M \cdot \frac{1}{4} \left(2 + \frac{\sigma_Y - \sigma_n}{\sigma_{\max}} \right) \left(1 - \frac{\sigma_Y - \sigma_n}{\sigma_{\max}} \right)^2$$

and equation (8) gives

$$M_R = M \cdot \left[1 - \frac{1}{4} \left(2 + \frac{\sigma_Y - \sigma_n}{\sigma_{\max}} \right) \left(1 - \frac{\sigma_Y - \sigma_n}{\sigma_{\max}} \right)^2 \right]$$

As deflection is proportional to bending moment, it results that

$$\delta_R = \begin{cases} \delta_T & \text{if } \frac{\sigma_Y - \sigma_n}{\sigma_{\max}} \geq 1 \\ \delta_T \cdot \left[1 - \frac{1}{4} \left(2 + \frac{\sigma_Y - \sigma_n}{\sigma_{\max}} \right) \left(1 - \frac{\sigma_Y - \sigma_n}{\sigma_{\max}} \right)^2 \right] & \text{if } \frac{\sigma_Y - \sigma_n}{\sigma_{\max}} < 1 \end{cases}$$

The parameter that indicates the onset of plastic deformation can be expressed as a function of h :

$$c = \frac{\sigma_Y - \sigma_n}{\sigma_{\max}} = \frac{a \cdot E\alpha(T_g - T_c) - E\alpha(T_g - T_c) \frac{h_0}{h}}{3E\alpha(T_g - T_c) \frac{h_0}{h} \left(1 - \frac{h_0}{h} \right)} = \frac{a - \frac{h_0}{h}}{3 \frac{h_0}{h} \left(1 - \frac{h_0}{h} \right)}$$

The yielding condition is

$$c < 1 \rightarrow a \left(\frac{h}{h_0} \right)^2 - 4 \frac{h}{h_0} + 3 < 0 \quad (9)$$

Solving inequality (9) and excluding the solution with $h < h_0$, it results that permanent deformation only occurs under the following threshold on part height:

$$\frac{h}{h_0} < \frac{2 + \sqrt{4 - 3a}}{a} = \frac{(2 + \sqrt{4 - 3a})(2 - \sqrt{4 - 3a})}{a(2 - \sqrt{4 - 3a})} = \frac{4 - 4 + 3a}{a(2 - \sqrt{4 - 3a})} = \frac{3}{2 - \sqrt{4 - 3a}}$$

and provided that $a < 4/3 = 1.33$.

6.3 Deflection equation

According to the above calculations, the residual deflection due to warpage can be estimated by the following equation, assumed valid for flat rectangular plates with $h > m \Delta h$:

$$\delta_R = \frac{3}{4} \alpha (T_g - T_c) \frac{l^2 m \Delta h}{h^2} \left(1 - \frac{m \Delta h}{h} \right) \cdot f(h, \Delta h, m, a) \quad (10)$$

where

$$f(h, \Delta h, m, a) = \begin{cases} 1 & \text{if } a \geq \frac{4}{3} \\ 1 & \text{if } a < \frac{4}{3}, h \geq \frac{3m\Delta h}{2 - \sqrt{4 - 3a}} \\ 1 - \frac{1}{4} (2 + c)(1 - c)^2, c = \frac{a - b}{3b(1 - b)}, b = \frac{m\Delta h}{h} & \text{if } a < \frac{4}{3}, h < \frac{3m\Delta h}{2 - \sqrt{4 - 3a}} \end{cases}$$

To illustrate the properties of the proposed analytic model, Fig. 11 shows how the estimated deflection changes with h on ABS parts with $l = 100$ mm and $\Delta h = 0.254$ mm. Material properties have been set to either average values within their expected ranges ($\alpha = 60 \cdot 10^{-6} \text{ K}^{-1}$, $E = 1500$ MPa, $\sigma_Y = 1.5$ MPa, $T_g = 95^\circ\text{C}$) or known process conditions ($T_m = 270^\circ\text{C}$, $T_c = 75^\circ\text{C}$). From equations (4) and (6), material-related parameters are thus

equal to $m = 4.72$ and $a = 0.83$. The residual deflection calculated by equation (10) is compared with those calculated by equation (3) from the elastic model with single-layer shrinkage, and by equation (5) from the elastic model with multiple-layer shrinkage. The following observations can be made about the incremental effects of the different hypotheses:

- The occurrence of multiple-layer shrinkage involves two main differences from the basic assumption of single-layer shrinkage. First, deflections are larger at equal heights, as it was obviously expected because of the greater extension of thermal stresses. Secondly, the rate of change of deflection when the height decreases does not grow hyperbolically, but slows down until deflection reaches a maximum ($h \approx 1.7$ mm in this case). This can be explained considering that, when shrinkage occurs in a sufficiently large fraction of part volume, the reaction force of the platform is closer to the neutral axis and its torque begins to decrease.
- The onset of plastic deformation leads to smaller deflections for part heights below a given threshold ($h \approx 4.3$ mm). As a possible explanation, at smaller heights the thermal stresses during the build process are more likely to exceed the elastic range and cause a permanent deformation, which reduces the residual deflection when the constraint of the platform is removed. As a side effect, the maximum deflection occurs for slightly thicker parts compared to the elastic case ($h \approx 2$ mm).

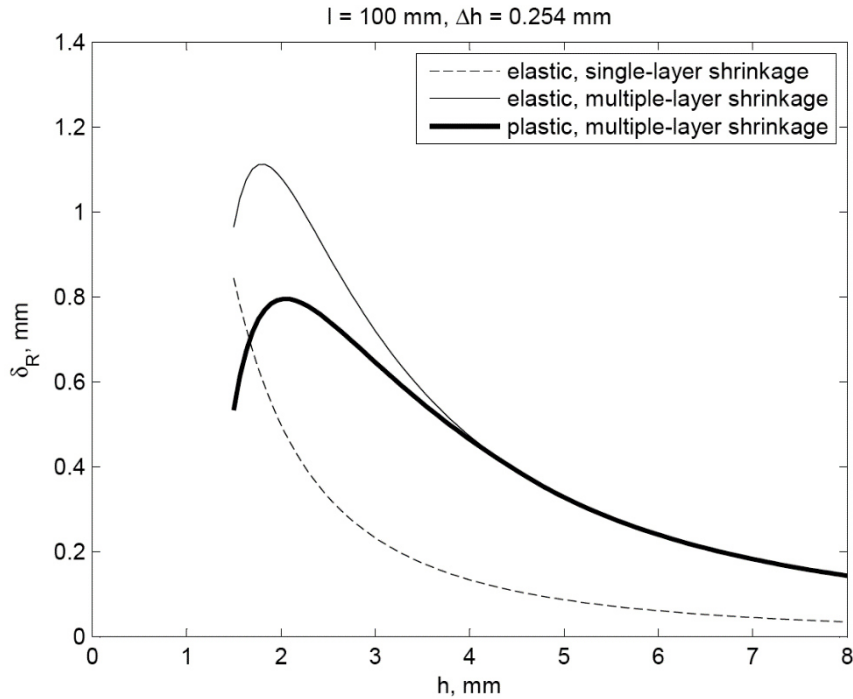


Fig. 11: Comparison of analytic models for warpage estimation

From the above considerations, both hypotheses seem to be relevant to an improved explanation of the warpage phenomenon compared to existing 1D models. At current stage, however, the proposed analytic model cannot be rigorously validated on experimental data, because it includes material parameters for which experimental data are not yet available. For demonstrative purposes, Fig. 12 shows a possible fitting of equation (10) to the experimental data of Tab. 5 with the following tuning operations:

- the material parameters have been set to best-fit values in their ranges ($\alpha = 40 \cdot 10^{-6} \text{ K}^{-1}$, $E = 1800 \text{ MPa}$, $\sigma_Y = 1 \text{ MPa}$);
- the warpage deflection has been converted into a flatness error to be compared with experimental data by the following correction:

$$\delta = c_0 + c_1 \Delta h + \delta_R$$

where δ_R is the distortion estimated from equation (10), $c_1 \Delta h$ is an estimate of the flatness errors due to intra-bead grooves, and c_0 is a constant error associated to disturbance factors not considered in the model; the correction parameters have been tentatively set to $c_0 = 0.1$ mm and $c_1 = 0.7$.

The analytic model captures both the effect of h (the decreasing rate of change of distortion with decreasing height) and the interaction between h and Δh (the occurrence or not of a maximum distortion according to layer thickness).

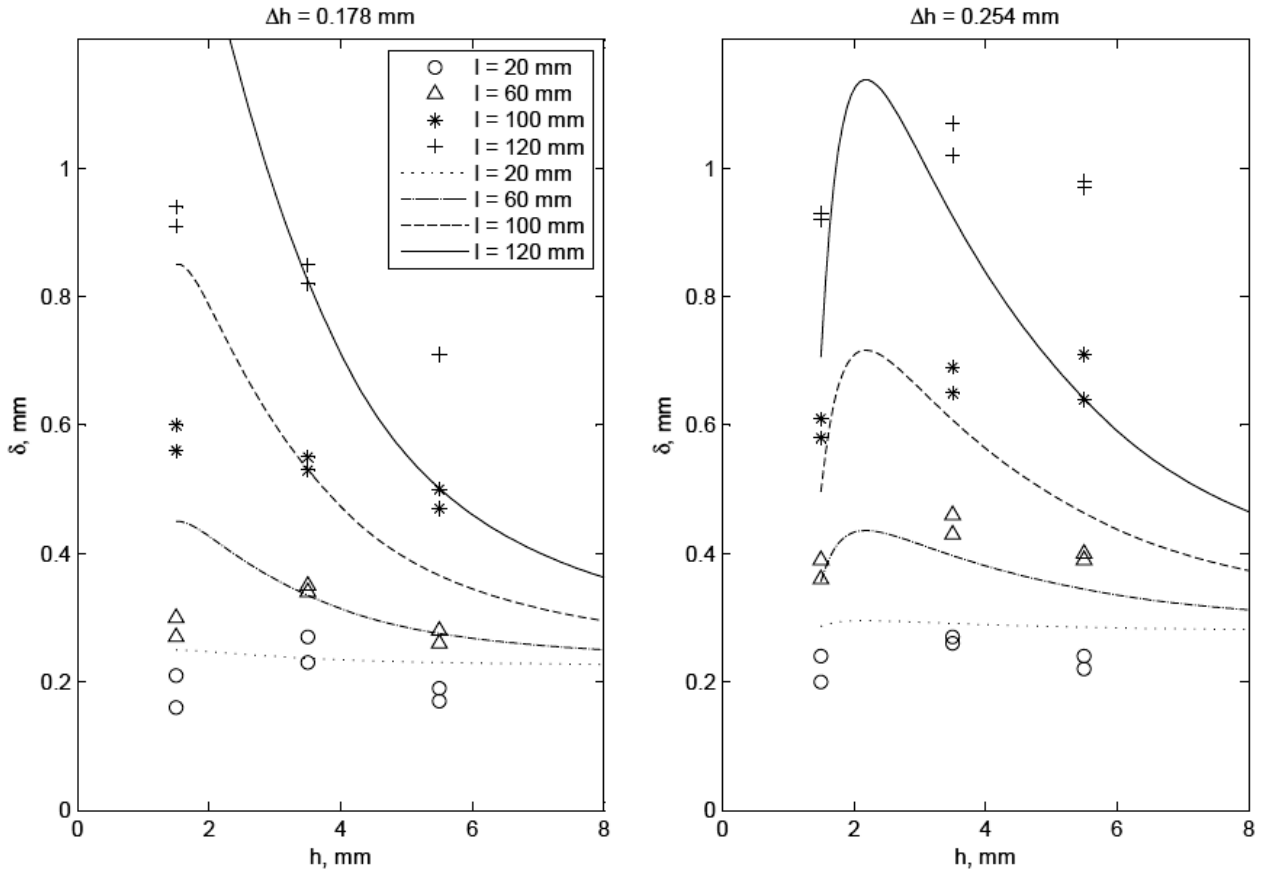


Fig. 12: Comparison between analytic model and experimental data: a) $\Delta h = 0.178$ mm, b) $\Delta h = 0.254$ mm

Despite the tuning, however, the model fits rather inaccurately to actual geometrical errors. This can also be noted in Fig. 13, which compares the experimental values of δ (δ_{exp}) with those given by the analytic model (δ_{mod}), reporting their linear regression with a 95% confidence interval. On the whole dataset, the model has a large error (about 1/3 of the total sum of squares) and a severe lack of fit (99% of the residual sum of squares). The model gives an especially poor fit for long and thick parts (which distort more than it is estimated), as well as for thin parts built with small layer thickness (where the distortion is considerably overestimated). The model will have to be revised considering additional physical mechanisms not considered in the present study.

7 Conclusions

The experimental results reported in this paper have allowed to verify and explain some known basic facts about warpage. For rectangular plates in ABS built by the FDM technique, thermal distortions are largely dependent on the maximum dimension on the horizontal plane, which seems to have a similar role to the length of a beam deflecting under a uniform bending moment. The choice of increasing layer thickness to reduce build time, which is known to impose compromises on surface finish, has also a moderate effect on warpage

because a larger volume of material is subjected to shrinkage during the thermal transient following the deposition of a new layer. Although this volume also depends on the transverse dimension of the plate, the latter does not significantly influence the amount of warpage because its increase makes the part more resistant to bending.

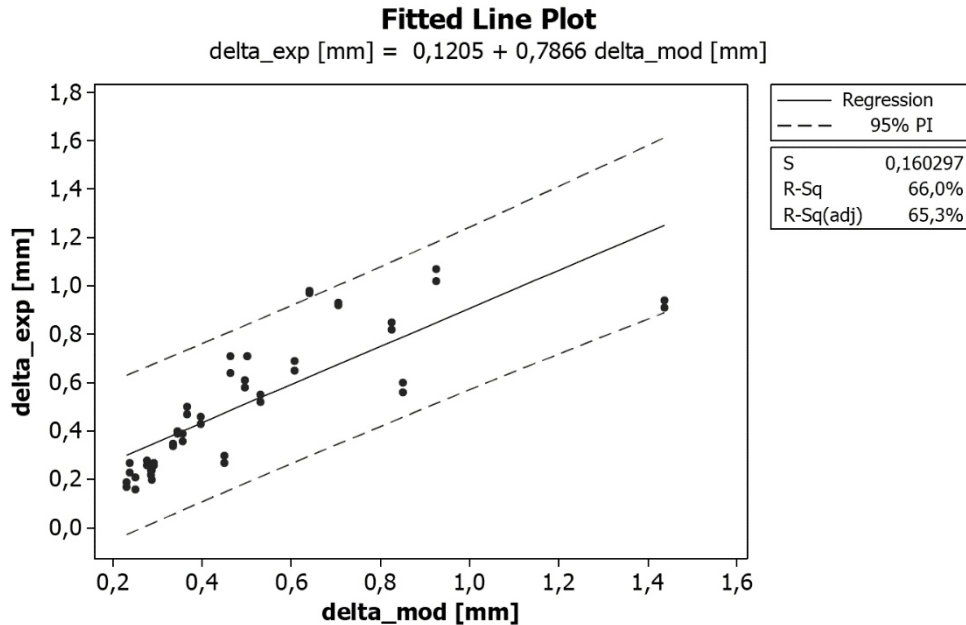


Fig. 13: Goodness-of-fit of the tuned model to the experimental data

About the influence of part height, test results suggest a different interpretation from literature. At a first approximation, a lower dimension along build direction leads to lower bending stiffness and thus to larger distortions. However, this effect seems to be predominant only before a maximum amount of warpage is reached at height values in the 2-4 mm range, while smaller distortions are observed for thinner parts. To explain this behavior, additional mechanisms need to be involved in the interpretation of warpage. This work has proposed two possible interpretations of why very thin parts distort less. The first one is the extension of shrinkage on multiple layers due to the thermal conduction through the part, which leads to a reduction of the total torque of thermal stresses. The second one is the permanent deformation of the material under bending stresses, which contributes to keep the part flat on the build platform but is not recovered as distortion as it is the case of elastic deformation. By a 1D analytic model of part distortion, these hypotheses have been shown to actually explain the peculiar influence of part height under common settings for materials and process parameters.

This work is based on very restrictive assumptions on the process, the material and the geometry of parts. Yet they help to improve the understanding of the physical causes of warpage, which is a key objective in order to investigate on the role of other variables beside the one considered here. Having paid special attention to part dimensions, the results of the paper may lead to further insights on what geometric features are critical for warpage even on parts with different shapes, such as flat parts with complex profiles. Future studies on increasingly complex part geometries could pave the way for the development of design-for-manufacture rules for FDM parts, with the objective of controlling accuracy issues since the phases of part design and process planning.

Acknowledgments

The authors are grateful to Timothy Minton (Brunel University) for his help and advice.

Compliance with ethical standards

This research did not receive any specific grant from funding agencies in the public, commercial, or not-for-profit sectors. The authors declare that they have no conflict of interest.

References

- [1] B.N. Turner, S.A. Gold, A review of melt extrusion additive manufacturing processes: II. Materials, dimensional accuracy and surface roughness, *Rapid Prototyp. J.* 21-3 (2015) 250-261.
- [2] P.H. Lee, H. Chung, S.W. Lee, J. Yoo, J. Ko, Review: dimensional accuracy in additive manufacturing processes, *Proc. ASME Int. Manuf. Sci. Eng. Conf.*, Detroit MI (2014), MSEC2014-4037.
- [3] O.A. Mohamed, S.H. Masood, J.L. Bhowmik, Optimization of fused deposition modeling process parameters: a review of current research and future prospects, *Adv. Manuf.* 3 (2015) 42-5.
- [4] R. Ippolito, L. Iuliano, A. Gatto, Benchmarking of rapid prototyping techniques in terms of dimensional accuracy and surface finish, *Ann. CIRP* 44-1 (1995) 157-160.
- [5] C.W. Ziemian, P.M. Crawn III, Computer aided decision support for fused deposition modeling, *Rapid Prototyp. J.* 7-3 (2001) 138-147.
- [6] C.J.L. Pérez, Analysis of the surface roughness and dimensional accuracy capability of fused deposition modelling processes, *Int. J. Prod. Res.* 40-12 (2002) 2865-2881.
- [7] T. Grimm, Fused deposition modeling: a technology evaluation, T.A. Grimm and Associates (2002).
- [8] C.C. Wang, T.W. Lin, S.S. Hu, Optimizing the rapid prototyping process by integrating the Taguchi method with the Gray relational analysis, *Rapid Prototyp. J.* 13-5 (2007) 304-315.
- [9] A. Noriega, D. Blanco, B.J. Alvarez, A. Garcia, Dimensional accuracy improvement of FDM square cross-section parts using artificial neural networks and an optimization algorithm, *Int. J. Adv. Manuf. Technol.* 69 (2013) 2301-2313.
- [10] R. Singh, Some investigations for small-sized product fabrication with FDM for plastic components, *Rapid Prototyp. J.* 19-1 (2013) 58-63.
- [11] R. Singh, Process capability analysis of fused deposition modelling for plastic components, *Rapid Prototyp. J.* 20-1 (2014) 69-76.
- [12] W.J. Johnson, M. Rowell, B. Deason, M. Eubanks, Comparative evaluation of an open-source FDM system, *Rapid Prototyp. J.* 20-3 (2014) 205-214.
- [13] L.M. Galantucci, I. Bodi, J. Kacani, F. Lavecchia, Analysis of dimensional performance for a 3D open-source printer based on fused deposition modeling technique, *Procedia CIRP* 28 (2015) 82-87.
- [14] A.K. Sood, R.K. Ohdar, S.S. Mahapatra, Improving dimensional accuracy of fused deposition modelling processed part using grey Taguchi method, *Mater. Des.* 30 (2009) 4243-4252.
- [15] A.K. Sood, R.K. Ohdar, S.S. Mahapatra, Parametric appraisal of fused deposition modelling process using the grey Taguchi method, *Proc. IMechE Part B J. Eng. Manuf.* 224 (2009) 135-145.
- [16] G.A.O. Adam, D. Zimmer, On design for additive manufacturing: evaluating geometrical limitations, *Rapid Prototyp. J.* 21-6 (2015) 662-670.
- [17] O.A. Mohamed, S.H. Masood, J.L. Bhowmik, Optimization of fused deposition modeling process parameters for dimensional accuracy using I-optimality criterion, *Meas.* 81 (2016) 174-196.
- [18] P. Fudali, W. Witkowski, D. Wydrzynski, Comparison of geometric precision of plastic components made by subtractive and additive methods, *Adv. Sci. Technol. Res. J.* 7-19 (2013) 36-40.
- [19] P.J. Nuñez, A. Rivas, E. Garcia-Plaza, E. Beamud, A. Sanz-Lobera, Dimensional and surface texture characterization in fused deposition modelling (FDM) with ABS plus, *Procedia Eng.* 132 (2015) 856-863.
- [20] P. Minetola, L. Iuliano, G. Marchiandi, Benchmarking of FDM machines through part quality using IT grades, *Procedia CIRP* 41 (2016) 1027-1032.

- [21] S. Mahmood, D. Talamona, K.L. Goh, A.J. Qureshi, Fast deviation simulation for fused deposition modeling process, *Procedia CIRP* 43 (2016) 327-332.
- [22] S. Agrawal, S.G. Dhande, Analysis of mechanical error in a fused deposition process using a stochastic approach, *Int. J. Prod. Res.* 45-17 (2007) 3991-4012.
- [23] K. Tong, S. Joshi, E.A. Lehtihet, Error compensation for fused deposition modeling (FDM) machine by correcting slice files, *Rapid Prototyp. J.* 14-1 (2008) 4-14.
- [24] L. Bochmann, C. Bayley, M. Helu, R. Transchel, K. Wegener, D. Dornfeld, Understanding error generation in fused deposition modeling, *Surf. Topogr. Metrol. Prop.*, 3 (2015) 014002.
- [25] A. Boschetto, L. Bottini, Accuracy prediction in fused deposition modeling, *Int. J. Adv. Manuf. Technol.* 73 (2014) 913-928.
- [26] A. Boschetto, L. Bottini, Triangular mesh offset aiming to enhance fused deposition modeling accuracy, *Int. J. Adv. Manuf. Technol.* 80 (2015) 99-111
- [27] A. Boschetto, L. Bottini, Design for manufacturing of surfaces to improve accuracy in fused deposition modeling, *Robot. Comput. Integr. Manuf.* 37 (2016) 103-114.
- [28] D.Y. Chang, B.H. Huang, Studies on profile error and extruding aperture for the RP parts using the fused deposition modeling process, *Int. J. Adv. Manuf. Technol.* 53 (2011) 1027-1037.
- [29] A. Ghazanfari, W. Li, M.C. Leu, R.G. Landers, Planning freeform extrusion fabrication processes with consideration of horizontal staircase effect, *Proc. Solid Freeform Fabrication Symp., Austin TX* (2015) 1313-1323.
- [30] A. Ghazanfari, W. Li, M.C. Leu, R.G. Landers, Optimal rastering orientation in freeform extrusion fabrication processes, *Proc. Solid Freeform Fabrication Symp., Austin TX* (2015) 1324-1333
- [31] J.S.S. Chen, H.Y. Feng, Contour generation for layered manufacturing with reduced part distortion, *Int. J. Adv. Manuf. Technol.* 53 (2011) 1103-1113.
- [32] N. Volpato, J.A. Foggiatto, D.C. Schwarz, The influence of support base on FDM accuracy in Z, *Rapid Prototyp. J.* 20-3 (2014) 182-191.
- [33] Q. Dao, J.C. Frimodig, H.N. Le, X.Z. Li, S.B. Putnam, K. Golda, J. Foyos, R. Noorani, B. Fritz, Calculation of shrinkage compensation factors for rapid prototyping (FDM 1650), *Comput. Appl. Eng. Educ.* 7 (1999) 186-195.
- [34] S.N.A.M. Halidi, J. Abdullah, Moisture effects on the ABS used for fused deposition modeling rapid prototyping machine, *IEEE Symp. Humanit. Sci. Eng. Res., Kuala Lumpur, Malaysia* (2012).
- [35] P. Jacobs, The effects of random noise shrinkage on rapid tooling accuracy, *Mater. Des.* 21 (2000) 127-136.
- [36] Coefficient of thermal expansion test report, *Stratasys, Eden Prairie MN* (2011).
- [37] S.N. Economidou, D. Karalekas, Optical sensor-based measurements of thermal expansion coefficient in additive manufacturing, *Polym. Test.* 51 (2016) 117-121.
- [38] A. Kantaros, D. Karalekas, In-situ monitoring of strain build up and temperature in a 3D polymer printing process, *Proc. Int. Conf. Exp. Mech., Cambridge, UK* (2014).
- [39] M. Mahesh, Y.S. Wong, J.Y.H. Fuh, H.T. Loh, Benchmarking for comparative evaluation of RP systems and processes, *Rapid Prototyp. J.* 10-2 (2004) 123-135.
- [40] A. Kantaros, D. Karalekas, Fiber Bragg grating based investigation of residual strains in ABS parts fabricated by fused deposition modeling process, *Mater. Des.* 50 (2013) 44-50.
- [41] A. Kantaros, J. Giannatsis, D. Karalekas, A novel strategy for the incorporation of optical sensors in fused deposition modeling parts, *Proc. Int. Conf. Adv. Manuf. Eng. Technol., Stockolm, Sweden* (2013) 163-170.
- [42] B.A. Boley, J.H. Wiener, *Theory of thermal stresses.* Dover, Mineola NY, 1998.
- [43] T.M. Wang, J.T. Xi, Y. Jin, A model research for prototype warp deformation in the FDM process, *Int. J. Adv. Manuf. Technol.* 33 (2007) 1087-1096.
- [44] G. Percoco, L.M. Galantucci, F. Lavecchia, Validation study of an analytical model of FDM accuracy, *DAAM Int Sci Book* (2011) 585-592.

- [45] Z. Zhu, V. Dhokia, A. Nassehi, S.T. Newman, Investigation of part distortions as a result of hybrid manufacturing, *Robot. Comput. Integr. Manuf.* 37 (2016) 23-32.
- [46] L. Xinhua, L. Shengpeng, L. Zhou, Z. Xianhua, C. Xiaohu, W. Zhongbin, An investigation on distortion of PLA thin-plate part in the FDM process, *Int. J. Adv. Manuf. Technol.* 79-5 (2015) 1117-1126.
- [47] Y. Zhang, Y.K. Chou, Three-dimensional finite element analysis simulations of the fused deposition modelling process, *Proc. IMechE Part B J. Eng. Manuf.* 220 (2006) 1663-1671.
- [48] Y. Zhang, K. Chou, A parametric study of part distortions in fused deposition modelling using three-dimensional finite element analysis, *Proc. IMechE Part B J. Eng. Manuf.* 222 (2008) 959-967.
- [49] A. Peng, X. Xiao, R. Yue, Process parameter optimization for fused deposition modeling using response surface methodology combined with fuzzy inference system, *Int. J. Adv. Manuf. Technol.* 73 (2014) 87-100.
- [50] A. Guerrero-de-Mier, M.M. Espinosa, M. Dominguez, Bricking: a new slicing method to reduce warping, *Procedia Eng.* 132 (2015) 126-131.
- [51] K.W. Dalgarno, T.H.C. Childs, I. Rowntree, L. Rothwell, Finite element analysis of curl development in the selective laser sintering process, *Proc. Solid Freeform Fabrication Symp.*, Austin TX (1996) 559-566.
- [52] H.J. Yang, P.J. Hwang, S.H. Lee, A study on shrinkage compensation of the SLS process by using the Taguchi method, *Int. J. Mach. Tool. Manuf.* 42 (2002) 1203-1212.
- [53] M. Held, C. Pfligersdorffer, Correcting warpage of laser-sintered parts by means of a surface-based inverse deformation algorithm, *Eng. Comput.* 25 (2009) 389-395.
- [54] A. Amado, M. Schmid, K. Wegener, Simulation of warpage induced by non-isothermal crystallization of co-polypropylene during the SLS process, *AIP Conf. Proc.* 1664 (2005) 160002.
- [55] G. Bugada, M. Cervera, G. Lombarda, E. Oñate, Numerical analysis of stereolithography processes using the finite element method, *Rapid Prototyp. J.* 1-2 (1995) 13-23.
- [56] B. Wiedemann, K.H. Dusel, J. Eschl, Investigation into the influence of material and process on part distortion, *Rapid Prototyp. J.* 1-3 (1995) 17-22.
- [57] M. Vatani, F. Barazandeh, A. Rahimi, A.S. Nezhad, Distortion modeling of SL parts by classical lamination theory, *Rapid Prototyp. J.* 18-3 (2012) 188-193.
- [58] K. Xu, Y. Chen, Deformation control based on in-situ sensors for mask projection based stereolithography, *Proc. ASME Int. Manuf. Sci. Eng. Conf.*, Detroit MI (2014) MSEC2014-4055.
- [59] C. Schmutzler, A. Zimmermann, M.F. Zaeh, Compensating warpage of 3D printed parts using free-form deformation, *Procedia CIRP* 41 (2016) 1017-1022.
- [60] ABSplus-P430 technical specifications, Stratasys, Eden Prairie MN (2016).
- [61] K. Carr, P. Ferreira, Verification of form tolerances Part I: basic issues, flatness, and straightness, *Precis. Eng.* 17 (1995) 131-143.
- [62] D.C. Montgomery, *Design and analysis of experiments*, 5th Ed, Wiley, New York, 2000.
- [63] C. Bellehumeur, L. Li, Q. Sun, P. Gu, Modeling of bond formation between polymer filaments in the fused deposition modeling process, *J. Manuf. Proc.* 6-2 (2004) 170-178.
- [64] T.A. Osswald, G. Menges, *Material science of polymers for Engineers*, 2nd Ed, Hanser, Munich, 2003.
- [65] P. Brindley, R. Goodridge, M. East, R. Hague, Preliminary investigation into the mechanical properties of Stratasys polycarbonate and M30 ABS materials, *Tech. Rep.*, Loughborough University (2008).
- [66] H.S. Carslaw, J.C. Jaeger, *Conduction of heat in solids*, Oxford University Press, London, 1959.

List of figures

Fig. 1: Warpage in the FDM process

Fig. 2: Fabrication of sample parts: a) part geometry; b) deposition strategy

Fig. 3: Warpage evaluation: a) measurement of parts; b) flatness error

Fig. 4: Individual effects of part dimensions

Fig. 5: Individual effects of length, height and layer thickness

Fig. 6: One-dimensional illustration of warpage

Fig. 7: Shrinkage on multiple layers

Fig. 8: Development of warpage after build: a) with elastic deformation; b) with permanent deformation

Fig. 9: Heat transient model for the calculation of shrinkage volume thickness

Fig. 10: Simplified stress pattern in the presence of plastic deformation

Fig. 11: Comparison of analytic models for warpage estimation

Fig. 12: Comparison between analytic model and experimental data: a) $\Delta h = 0.178$ mm, b) $\Delta h = 0.254$ mm

Fig. 13: Goodness-of-fit of the tuned model to the experimental data

List of tables

Tab. 1: Factors and levels of the first experiment

Tab. 2: Warpage measured with different combinations of part dimensions

Tab. 3: ANOVA of warpage with respect to part dimensions

Tab. 4: Factors and levels of the second experiment

Tab. 5: Warpage measured with varying length, height and layer thickness

Tab. 6: ANOVA of warpage with respect to length, height and layer thickness